frontiers in Physics

TYPE Original Research
PUBLISHED 10 April 2026
DOI 10.3389/fphy.2026.1783743

Check for updates

OPEN ACCESS

EDITED BY
Ji Wang,
Ningbo University, China

REVIEWED BY
Longbiao Yan,
Beijing Urban Construction Design and Development Group Co., Ltd, China
Yanan Zhang,
Shenyang Ligong University, China

*CORRESPONDENCE
Xin Li,
lixin1924@nuaa.edu.cn

RECEIVED 08 January 2026
REVISED 14 March 2026
ACCEPTED 20 March 2026
PUBLISHED 10 April 2026

CITATION
Hu Z, Luo X, Zhang J, Li Q, Huang C, Lu C and Li X (2026) Research on AE method for thermal fatigue damage in heat transfer oil pipes.
Front. Phys. 14:1783743.
doi: 10.3389/fphy.2026.1783743

Research on AE method for thermal fatigue damage in heat transfer oil pipes

Zhenlong Hu[1,2], Xinxin Luo[3], Junjiao Zhang[1,2], Qiufeng Li[3], Changhui Huang[4], Chao Lu[3] and Xin Li[4]*

[1]China Special Equipment Inspection and Research Institute, Beijing, China, [2]Technology Innovation Center of Risk Prevention and Control of Refining and Chemical Equipment, State Administration for Market Regulation, Beijing, China, [3]Key Laboratory of Nondestructive Testing (Ministry of Education), Nanchang Hangkong University, Nanchang, China, [4]Special Equipment Inspection and Testing Institute of Jiangxi General Institute of Inspection, Testing and Certification, Nanchang, China

Thermal oil pipes in concentrated solar power systems face prevalent risks of thermal fatigue damage during long-term outdoor service, while the dynamic monitoring of such structures remains an unaddressed gap. This study develops a dynamic monitoring and evaluation method for thermal fatigue damage using acoustic emission (AE) technology. Firstly, three types of U-shaped specimens are designed and fabricated from 20# steel, considering the material and structural characteristics of actual heat transfer oil pipes. Secondly, an inner-wall thermal cycle loading device is developed to simulate the real service environment, aligning with the actual thermal fatigue stress mode of the pipes. Finally, an AE detection experimental system is established; thermal fatigue loads are applied to the specimens via the loading device, and AE detection experiments are conducted. The study focuses on analyzing AE characteristic parameters during two stages of thermal fatigue, establishing the intrinsic correlation between signals and the damage process, with results validated against X-ray detection. Findings indicate distinct differences in AE characteristics across damage stages: The initiation stage is dominated by low-energy signals, while energy significantly increase during the propagation stage, the average energy increment is approximately 4,200 kpJ. X-ray detection confirms the effectiveness and accuracy of AE technology in characterizing thermal fatigue damage. This research demonstrates the promising application of AE technology for monitoring thermal fatigue damage in heat transfer oil pipes, providing experimental and theoretical support for online monitoring and service life prediction of such critical components.

KEYWORDS

acoustic emission, characteristic parameters, hot cycle loading, thermal fatigue damage, thermal oil pipe

1 Introduction

Concentrated solar power (CSP) is an emerging clean and low-carbon energy technology that utilizes large-scale arrays of parabolic or dish-shaped mirrors to collect solar thermal energy. The captured heat is converted into steam through heat exchange systems, which then drives traditional steam turbines for power generation [1, 2]. Unlike intermittent renewable energy sources such as photovoltaic (PV) and wind power, CSP systems store heated water in large-scale tanks, enabling 24/7 stable power supply. This capability makes CSP a pivotal technology for constructing new power systems and holds strategic significance for countries pursuing carbon peaking and carbon neutrality goals [3, 4].

Heat transfer oil pipes serve as the core components of trough-type CSP systems, responsible for transporting heat transfer oil. They form the critical connection between the solar field (heat collection island), heat storage and exchange island, and power generation island, efficiently transferring thermal energy converted from solar radiation to either the storage system or directly to the power generation unit [5–7]. However, the Earth's rotation causes diurnal cycles in solar irradiation, leading to daily temperature fluctuations in the heat transfer oil pipes [8]. These pipes are typically subjected to thermal fatigue loads, and even thermal shock loads during shading events such as sandstorms, rain, or snow. Among all components, the heat transfer oil pipes at the outlet of vacuum collector tubes operate under the most severe conditions [9]. Currently, long-term operating pipes suffer from widespread thermal fatigue damage, with multiple cracking and leakage accidents reported globally. Nevertheless, research on non-destructive testing (NDT) and evaluation methods for such damage remains scarce.

In recent years, significant progress has been made in understanding the damage mechanisms of CSP components, including thermal fatigue, thermal ratcheting, and thermal shock. He et al. noted that receivers operate in extremely harsh environments with large surface temperature gradients, which can induce substantial thermal stress and even lead to tube rupture [10]. Du et al. investigated fatigue cracks in solar molten salt tower receivers and identified severe thermal ratcheting in typical molten salt temperature-stratified storage tanks. Cyclic operation causes repeated variations in thermal stress, resulting in fatigue fracture or damage at locations with high stress or strain concentrations [11]. Janssens KGF et al. developed a low-cycle fatigue damage criterion using finite element analysis coupled with temperature-material plastic hardening effects to assess the cyclic thermal shock life of structural components [12]. Despite these advances, effective high-temperature online detection and evaluation methods for such damages remain underdeveloped.

Acoustic emission (AE) is a non-destructive monitoring technology that detects, evaluates, and locates dynamic defects in materials or structures by capturing transient elastic waves generated during deformation or fracture [13]. Currently, AE technology is predominantly applied to room-temperature equipment, with limited research conducted under high-temperature conditions. Jin et al. utilized AE to reveal interfacial defect characteristics between the oxide film and substrate during the high-temperature oxidation of Co-40Cr alloys [14]. He Kuanfang et al. explored the key characteristics and challenges of online AE detection for welding solidification hot cracks under cooling thermal shock, reviewed AE dynamic models, and discussed solutions for applying AE technology to high-temperature thermal fatigue crack detection in welding processes [15]. JIA et al. studied AE characteristics of damage behavior in industrial refractory materials under stress during high-temperature thermal cycles, finding that signal activity depends on the difference in thermal expansion coefficients between the matrix and inclusions, as well as the type of evolved cracks, with matrix microcracks exhibiting high AE signal activity [16]. Xu et al. applied AE technology to the damage diagnosis of thermal barrier coatings, analyzing mechanical properties and microstructural changes during high-temperature thermal fatigue experiments. Their research revealed that AE signal characteristics are independent of thermal fatigue cycle frequency but are primarily governed by crack derived modes [17]. These studies confirm the feasibility of AE technology for detecting and evaluating high-temperature thermal fatigue damage in materials. However, for online AE detection of thermal fatigue cracking in critical CSP components such as heat transfer oil pipes, in-depth analysis of AE signal characteristics during heating, high-temperature holding, and cooling stages is essential. Additionally, the influence of factors such as maximum temperature and temperature difference on thermal fatigue damage requires systematic investigation. Currently, research in this specific area remains lacking globally.

This study focuses on developing an AE monitoring method for thermal fatigue damage in in-service heat transfer oil pipes of CSP systems. Simulated specimens are designed based on the structure of actual pipes, and thermal fatigue loading is applied to the inner surface of specimens within 400 °C while maintaining the outer surface at ambient temperature to replicate real service conditions. During AE detection, high-temperature sensors are used to collect thermal fatigue damage signals. A parameter threshold method is explored for AE signal identification, effectively eliminating background noise and enabling dynamic signal collection and monitoring of crack initiation and propagation processes.

2 Theory of thermal fatigue damage and principles of AE detection

2.1 Theory of thermal fatigue damage

Rapid temperature fluctuations induce temperature gradients across the pipe cross-section, leading to uneven thermal expansion—a phenomenon particularly pronounced in thick-walled pipes. When the constraint stress resulting from uneven thermal expansion exceeds the material's yield strength, cracks initiate. Periodic temperature variations further accelerate crack propagation. Meanwhile, high-temperature environments induce microstructural changes in the pipe material, reducing fatigue resistance and promoting oxidation at the material surface and crack tips, which may even cause local melting, thereby accelerating thermal fatigue failure [18]. This phenomenon, where cyclic stress induced by temperature changes leads to material damage, is defined as thermal fatigue. Consequently, welds and elbows of heat transfer oil pipes are at high risk of thermal fatigue cracking.

The core mechanism of thermal fatigue damage theory lies in the generation of cyclic thermal stress when materials are subjected to periodic temperature changes and constrained from free expansion or contraction (either externally or internally). Repeated application of such thermal stress accumulates microdamage, ultimately leading to crack initiation, propagation, and complete material failure [19–21]. The primary objective of thermal fatigue experiments on heat transfer oil pipes is to evaluate material resistance to thermal fatigue. This is achieved by accurately replicating cyclic temperature variation characteristics of actual service conditions, reproducing real thermal stress cycles in test specimens, and systematically observing the entire process from microdamage accumulation to macroscale failure [22–24].

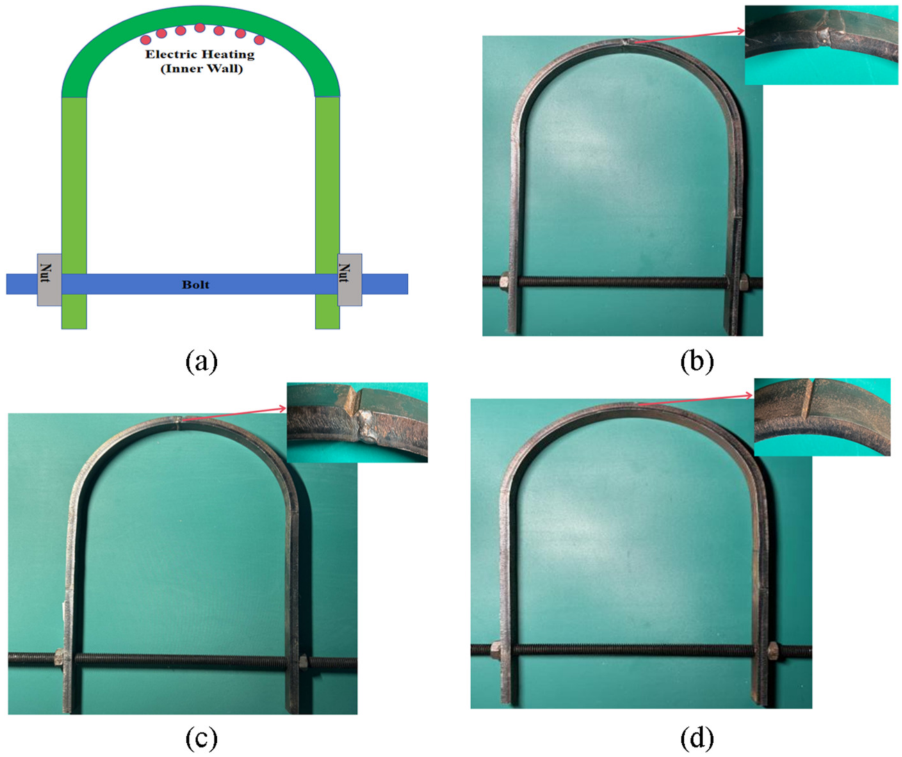

FIGURE 1
Structural diagrams of specimens.**(a)** Schematic diagram of specimen structure **(b)** Welded specimen (SY-1) **(c)** Welded specimen with V-shaped notch (SY-2) **(d)** Non-welded specimen with V-shaped notch (SY-3).

Synthetic heat transfer oils commonly used in CSP plants have a maximum allowable operating temperature ranging from 350 °C to 400 °C. To ensure heat transfer efficiency, the oil is operated near or at this upper limit during normal service. Due to the alternating effects of daytime and nighttime illumination, the temperature inside the heat transfer oil pipe will exhibit periodic fluctuations—dropping to approximately 150 °C at night and rising to 400 °C during the day. Therefore, a thermal cycle range of 150 °C–400 °C is selected for the experiments, which not only accurately reproduces the actual temperature variation pattern but also induces thermal stress cycles consistent with real service conditions [25].

2.2 Damage characterization based on AE characteristic parameters

The characteristic parameter analysis method for acoustic emission monitoring signals employs characteristic parameters of simplified waveforms to represent a certain amount of relevant information contained in acoustic emission signals, and further characterizes and analyzes the collected acoustic emission sources to achieve effective evaluation of defect information in acoustic emission testing [26, 27]. Common characteristic parameters of acoustic emission signals include hits, amplitude, counts, energy, duration, rise time, etc. Any signal that exceeds the threshold and enables a channel to acquire data is defined as a hit. Amplitude refers to the maximum amplitude value of the signal waveform. Counts represent the number of oscillations of the signal that cross the threshold. The area under the detected envelope of the signal is defined as energy. Duration is the time interval from the first threshold crossing of the signal to its final drop below the threshold. Rise time is the time interval from the first threshold crossing of the signal to the occurrence of the maximum amplitude [28–30].

3 Establishment of experimental testing system

3.1 Design and fabrication of specimens

20# steel is commonly used for manufacturing actual heat transfer oil pipes; therefore, this study designs and fabricates U-shaped bent loading specimens from 20# steel (Figure 1). Each specimen has a thickness of 6 mm, with both ends connected by bolts to simulate the stress state of in-service pipes. To further replicate the actual pipe structure and accelerate the thermal fatigue damage process, three types of U-shaped specimens are fabricated: welded specimens with V-shaped notches, welded specimens without notches, and non-welded specimens with V-shaped notches. One specimen of each type is subjected to thermal fatigue testing, designated as SY-1, SY-2, and SY-3 respectively.

20# steel is commonly adopted as the material for the actual fabrication of heat-conducting oil pipes. Accordingly, a U-shaped bending loading specimen was designed and prepared using 20# steel in this study (Figure 1). The length of the specimen is 600 mm,

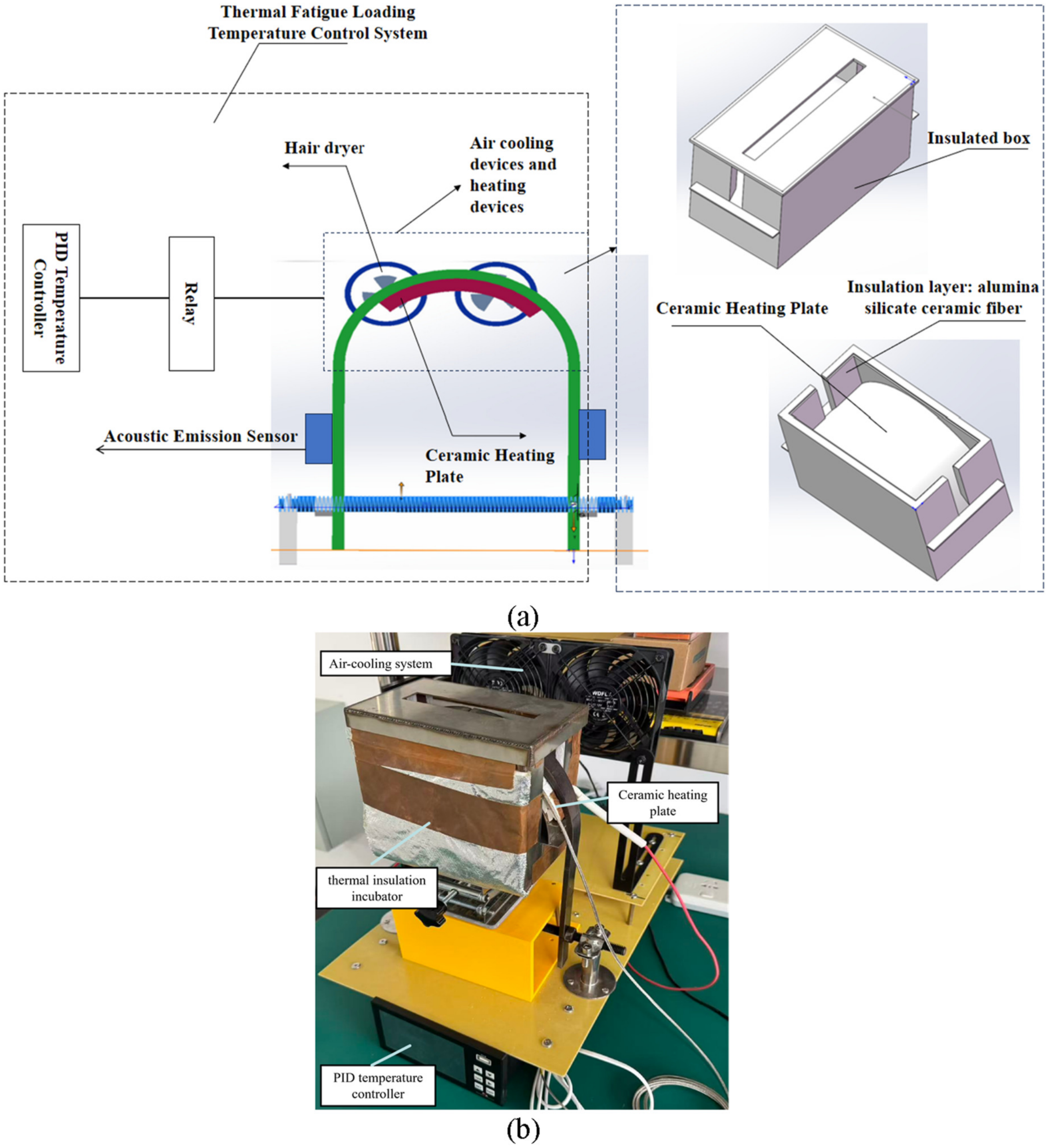

FIGURE 2
Structural diagrams of thermal fatigue cycle loading device and insulation box. **(a)** Structural diagram of thermal fatigue cycle loading device; **(b)** Physical picture of thermal fatigue cycle loading device.

and the specimen featured a bent section with an inner diameter of 95 mm, an outer diameter of 101 mm and a thickness of 6 mm, and its two ends were connected by bolts (with a bolt distance of 30 mm from the specimen end), which could simulate the stress state of heat-conducting oil pipes under actual service conditions to a certain extent. Acoustic emission sensors were mounted at 10 mm above the two bolts. To further mimic the actual structure of heat-conducting oil pipes and accelerate the thermal fatigue damage process, three types of U-shaped specimens were fabricated, namely the welded specimen with a 3 mm-deep V-shaped notch, the welded specimen without a notch, and the non-welded specimen with a V-shaped notch (60° Opening). One specimen of each type was subjected to thermal fatigue testing, numbered as SY-1, SY-2 and SY-3, respectively.

3.2 Development of thermal fatigue cycle loading device

In actual service, the outer wall of heat transfer oil pipes is typically exposed to air, while the inner wall undergoes thermal cycle loading during heat transfer. To simulate the actual thermal fatigue process, a custom

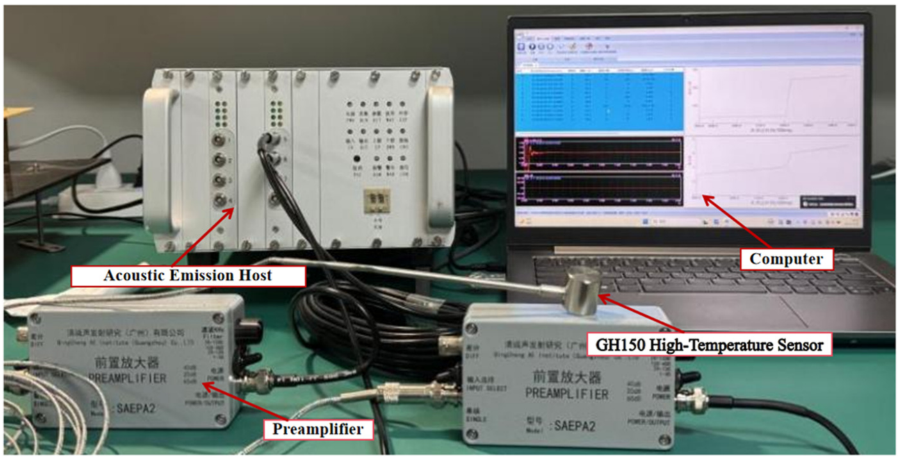

FIGURE 3
Physical diagram of SAEU3H digital acoustic emission detection system.

TABLE 1 **Acoustic emission acquisition parameters.**

Parameter threshold	Preamplifier gain	Hit lockout time	Peak definition time (PDT)	Hit definition time (HDT)
50 dB	40 dB	2000 μs	200 μs	1,000 μs

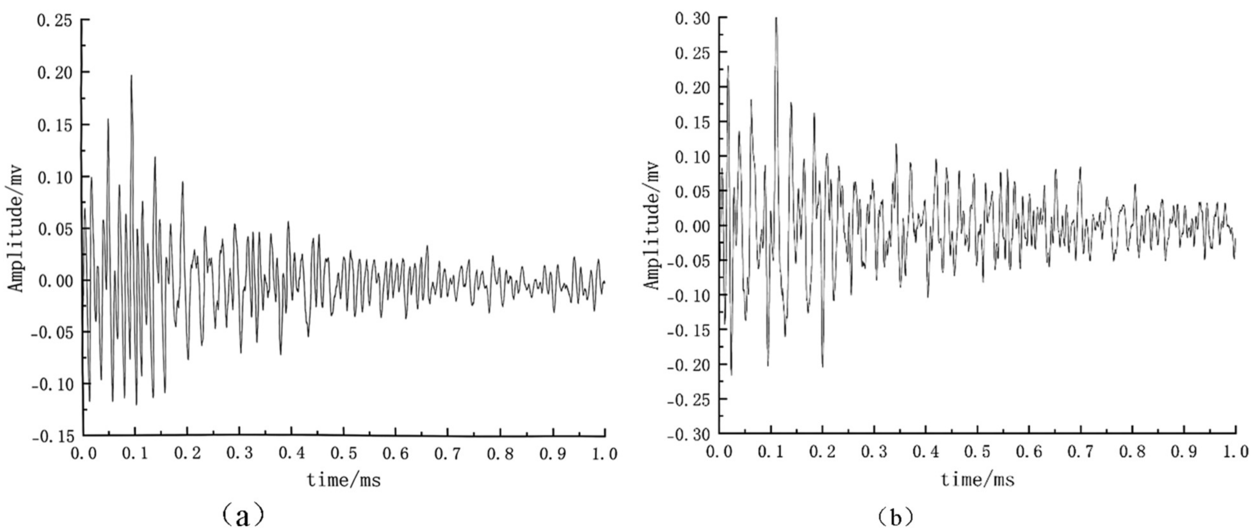

FIGURE 4
Waveform of pencil-lead break verification experiment. **(a)** Waveform of channel 5. **(b)** Waveform of channel 6.

inner-wall thermal cycle loading device is designed (Figure 2).

As shown in Figure 2, the specimen clamping module can fix the U-shaped specimen via the bolts at its two ends. Meanwhile, a 2000 W ceramic heating plate is attached to the curved inner wall of the U-shaped specimen for cyclic loading, which enables the rapid heating of the specimen's inner wall from room temperature to the experimentally set 400 °C, meeting the heating rate requirement for thermal fatigue cycling. Another core component of the thermal fatigue cyclic loading device is the temperature cyclic loading control module. In accordance with the actual temperature variation range of 150 °C–400 °Con the inner wall of heat-conducting oil pipes, a PID intelligent temperature controller is adopted for precise temperature regulation, with the heating time set freely. By pre-embedding K-type thermocouples (temperature measurement range: −20 °Cto 800 °C) in the stress-concentrated areas of the specimen's inner wall, real-time acquisition and closed-loop feedback control of temperature signals are realized, and the system can automatically record the complete temperature variation curve. Calibration through

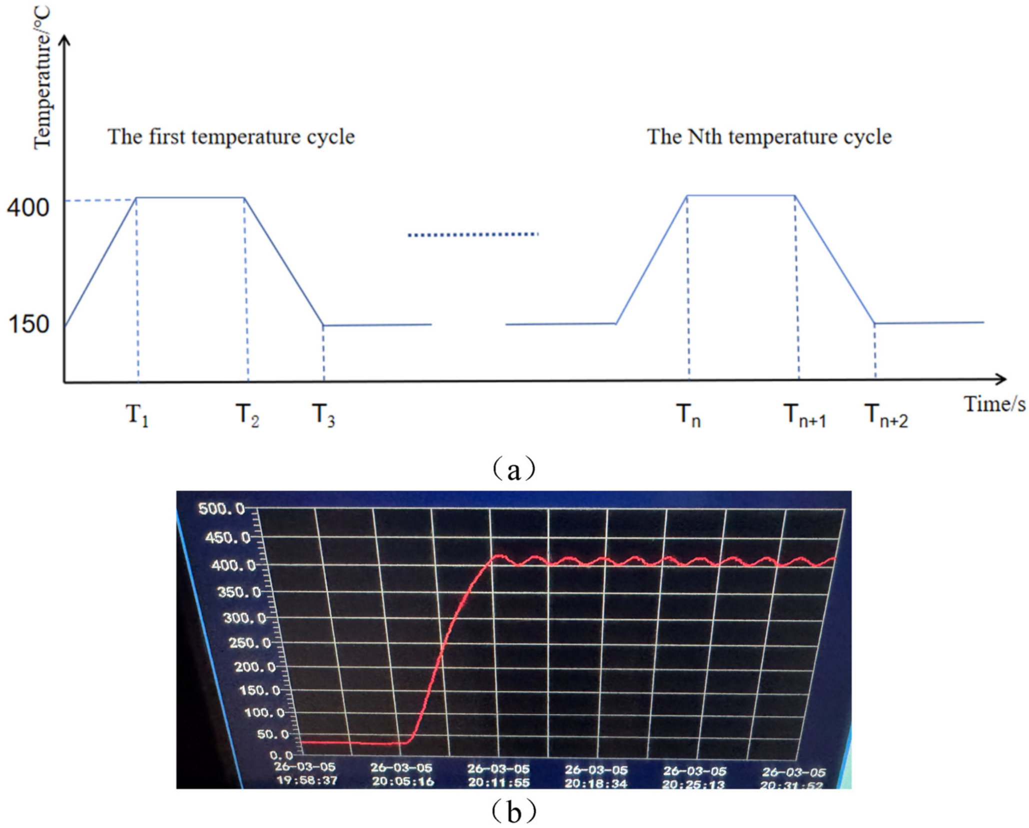

FIGURE 5
Schematic diagram of thermal fatigue temperature cycle loading process. **(a)** Temperature cycle loading design diagram; **(b)** Actual loading temperature curve graph.

multiple experiments has verified that the system fully meets the high-precision temperature control requirements of thermal fatigue experiments. For cooling, an air cooling method with fan blowing is adopted, with multi-gear adjustable wind speed. Practical measurements show that the method can rapidly cool the specimen's inner wall from 400 °C to 150 °C, which matches the actual cooling conditions of heat-conducting oil pipes in service and satisfies the experimental requirement for rapid cooling in thermal cycling.

Given the maximum inner wall temperature of 400 °C, a rectangular insulation box is specifically designed to cover the U-shaped specimen to ensure effective temperature control. As a core component for simulating the real service environment and ensuring reliable thermal fatigue tests, the insulation box features an outer layer made of 304 stainless steel and an inner quasi-hermetic space constructed from ceramic fiber boards. Ceramic fiber boards exhibit extremely low thermal conductivity, The core performance parameters of this ceramic fiber board are as follows: thermal conductivity ≤ 0.095 W/(m·K), long-term service temperature resistance ≥ 650 °C, bulk density 260–320 kg/m^3, and thickness 50 mm. It features a low thermal conductivity, effectively preventing heat loss from the hermetic space to the external environment and reducing thermal dissipation during heating. The hermetic space formed by the ceramic fiber boards creates a stable thermal environment, minimizing local temperature differences within the box and ensuring uniform heating of all specimen regions (especially the V-shaped notch at the top of the U-bend). This ensures that the applied thermal fatigue load matches the thermal load characteristics of pipes in real service.

To replicate the actual service condition of heat transfer oil pipes—where the inner wall is heated and the outer wall is exposed to air—the insulation box is designed with dedicated windows to allow the outer surface of the specimen to contact air. This creates a temperature difference structure of "hot inner surface and cold outer surface," ensuring consistency between the experimental environment and real service conditions, and making the initiation and propagation of thermal fatigue cracks more representative of actual scenarios.

3.3 Acoustic emission detection system

The SAEU3H AE system is employed in this study, featuring 8 channels configured with two data acquisition cards. This system enables functions such as analog signal acquisition, amplification, filtering, characteristic parameter extraction, and waveform display. GH150 high-temperature AE sensors are used, with a central frequency of 150 kHz, an effective receiving bandwidth of 60–400 kHz, and a maximum operating temperature of 600 °C (Figure 3). The specific acoustic emission acquisition parameters are shown in Table 1.

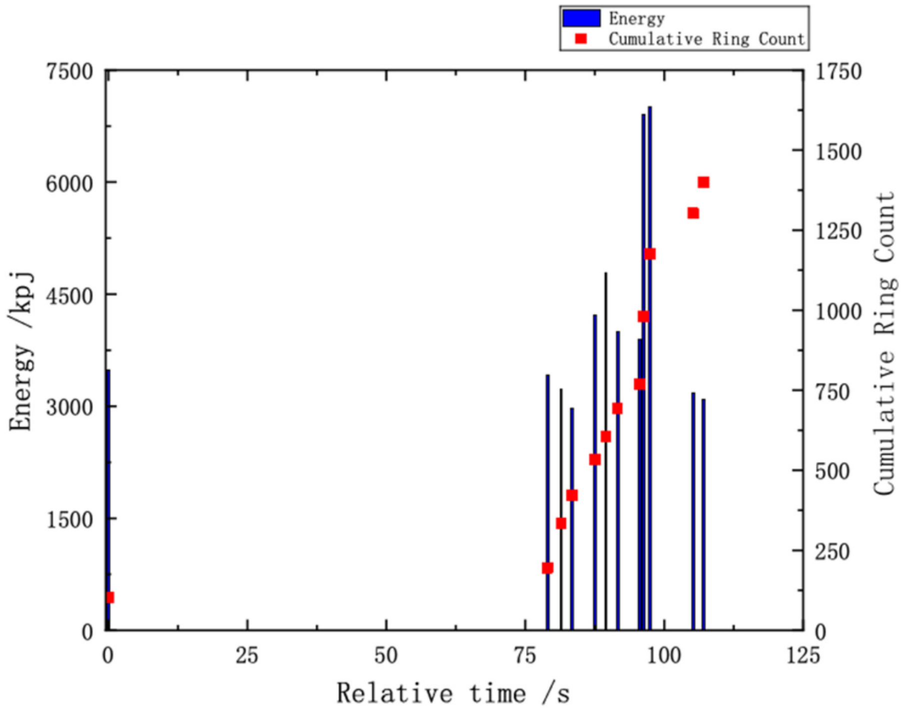

FIGURE 6
AE signal energy and cumulative ring count time-history curves of specimen SY-1 after the first stage of thermal fatigue cycles.

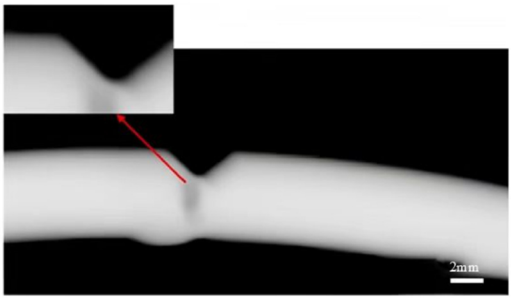

FIGURE 7
X-ray detection image of specimen SY-1.

AE sensors are symmetrically mounted on the surface of the U-shaped specimen as shown in Figure 2. To reduce noise interference and ensure good acoustic coupling, high-temperature silicone grease is applied between the AE sensors and the specimen surface, and the sensors are secured using probe clamps. Simulated testing is then conducted: AE signals released by the specimen during thermal fatigue are collected to analyze and characterize the material damage evolution process.

To verify the signal receiving consistency of the two AE sensors, standard lead-broken signals were used as the excitation source. Comparative tests were conducted under the same specimen, coupling conditions, and acquisition parameters. The results show that the waveforms received by the two sensors are highly coincident, the waveform is shown in Figure 4 which indicating that the two AE sensors have good receiving consistency and can be used for subsequent synchronous monitoring.

4 Experimental testing process and result analysis

4.1 Experimental process

Preparatory work is performed before each thermal fatigue experiment: (1) Comprehensive inspection of the U-shaped specimen, with the surface cleaned using industrial alcohol; (2) Installation of AE sensors at the positions shown in Figure 2, followed by lead-breaking tests to verify the sensitivity of each sensor and its ability to effectively receive AE signals from simulated damage locations; (3) Activation of the PID temperature controller power supply and configuration of temperature control parameters.

After completing the preparatory work, the AE detection system is officially started, and the temperature controller is activated to initiate thermal cycle loading on the inner wall of the U-shaped specimen. Since the inner wall of heat transfer oil pipes operates within the range of 150 °C–400 °C for long periods, the inner wall temperature is first heated to 150 °C, followed by four stages of temperature cycle loading as illustrated in Figure 5: Stage 1 (Heating): 150 °C–400 °C; Stage 2 (Insulation): 400 °C maintained for 5 min; Stage 3 (Cooling): 400 °C–150 °C; Stage 4 (Insulation): 150 °C maintained for 5 min. AE signals associated with damage are continuously monitored in real-time throughout the thermal fatigue process.

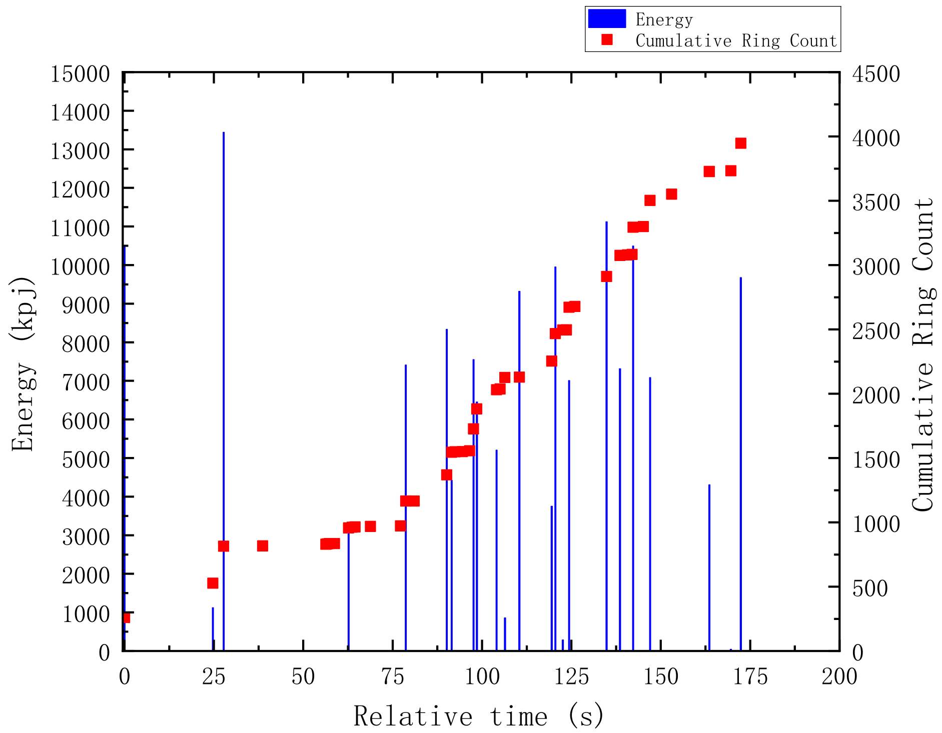

FIGURE 8
AE signal energy and cumulative ring count time-history curves of specimen SY-1 after the second stage of thermal fatigue cycles.

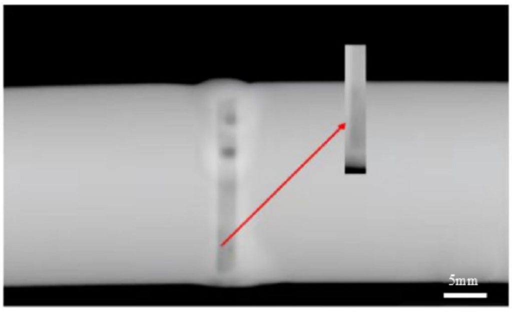

FIGURE 9
X-ray detection image of specimen SY-1 after the second stage of thermal fatigue cycles.

4.2 Result analysis

Each 100 temperature cycles are defined as one stage during the thermal fatigue process. The following analysis focuses on extracting AE signal characteristic parameters from two stages (200 total cycles) and evaluating damage by correlating with X-ray detection results.

4.2.1 AE signals from the first stage of cycles

Figure 6 presents the time-history curves of AE signal energy and cumulative ring count for specimen SY-1 during the 73rd heating cycle in the first stage. From the energy curve, it is observed that stress accumulates due to thermal expansion during the initial phase, with no substantial crack damage. Multiple peaks appear between 75–100 s, attributed to microcrack initiation and crack tip propagation as stress concentration within the material exceeds the critical threshold, resulting in significant energy release. After 100 s, the energy value decreases rapidly, indicating that the damage process stabilizes. High-temperature expansion of the heat transfer oil pipe material leads to crack closure under compressive stress.

The cumulative ringing count curve shows no significant increase in the initial phase, corresponding to weak background signals induced by elastic deformation of the material during the early thermal cycle stage, which do not contribute to actual damage. A steady increasing trend is observed between 75–100 s, with each damage event accompanied by stable signal duration, indicating consistent energy release during crack propagation. The slow growth after 100 s further confirms the termination of the damage process. No AE signals are detected from the other two specimens during this stage.

To confirm microcrack initiation in specimen SY-1, X-ray detection is performed on its top surface, The core parameters of the X-ray system are set as follows: tube voltage of 280 kV, tube current of 1.2 mA, and focal spot size of 0.4 mm. The detection was focused on the curved top and the welding zone of the specimen. With results shown in Figure 7. The image reveals a microcrack along the edge of a blowhole in the specimen.

4.2.2 AE signals from the second stage of cycles

Continue the second stage of 100 thermal fatigue cycle tests on the three samples with continuous AE signal monitoring. Specimen

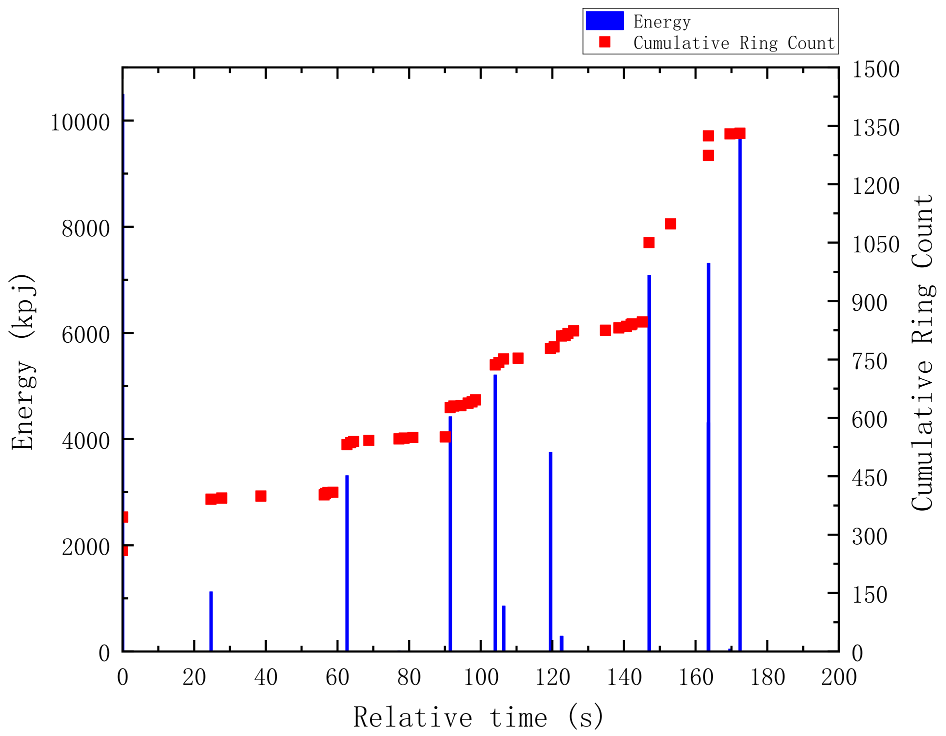

FIGURE 10
AE signal characteristic parameter time-history curves of specimen SY-2 after the second stage of thermal fatigue cycles.

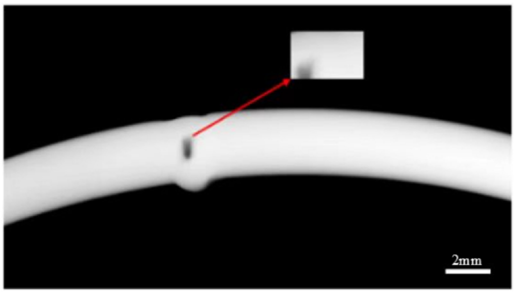

FIGURE 11
X-ray detection image of specimen SY-2 after the second stage of thermal fatigue cycles.

SY-1 generates AE signals again during the 43rd cooling cycle of the second stage; the time-history curves of AE signal amplitude and energy are presented in Figure 8.

As shown in Figure 8, numerous high-amplitude AE signals are generated during the cooling process, with multiple energy peaks exceeding 10,000 kpj (high-energy events). The high-energy signals collected during the 43rd thermal cycle of the second stage are primarily attributed to the microcracks initiated in the first stage. Thermal cycles in the second stage further drive crack expansion. Additionally, as a welded specimen with defects, cooling-induced material contraction is constrained during the cooling phase, leading to tensile stress concentration at grain boundaries. Welding defects exacerbate this stress, resulting in rapid crack propagation. X-ray detection is repeated on the specimen, with imaging performed from the upper end of the crack to enhance visibility (Figure 9). The crack is significantly more prominent compared to that observed in Figure 7.

Furthermore, AE signals are detected from specimen SY-2 during the 64th heating cycle of the second stage, despite no crack initiation observed in the first stage. The time-history curves of AE signal energy and cumulative count are shown in Figure 10. Significant fluctuations in AE signal energy are observed during the 64th heating cycle of the second stage, indicating the presence of strong AE sources. This is associated with mechanisms such as grain boundary sliding and phase transformation within the material. Although no macroscopic defects are present in the specimen, residual stress release or microscale dislocation motion may occur, leading to crack initiation.

To confirm crack initiation in specimen SY-2, X-ray detection is conducted on its top surface (Figure 11). The image shows that the length of microcracks initiated in specimen SY-2 is shorter than that initiated in specimen SY-1 during the first stage. No AE signals are detected from specimen SY-3 after the second stage of thermal fatigue cycles.

The above analysis demonstrates that AE signal characteristic parameters (e.g., amplitude, energy) of U-shaped specimens during thermal fatigue cycles effectively characterize the evolution of crack damage. AE signals corresponding to crack initiation are detected in specimens SY-1 and SY-2 during the two stages, with relatively low amplitude and energy, indicating the capability of AE technology to monitor early-stage damage signals. For specimen SY-1, the average acoustic emission energy increased from approximately 5,200 kpJ in the first test to 9,400 kpJ in the second test, with an increase of about 4,200 kpJ. This enables the identification and evaluation of damage stages through further characteristic analysis.

X-ray detection results are consistent with AE signal characteristics, confirming that AE detection can effectively characterize thermal fatigue damage and its severity. Additionally, crack initiation in specimens SY-1 and SY-2 occurs during the heating stage, indicating that the material is more prone to thermal fatigue damage under heating conditions. Special attention should be paid to the heating stage in future monitoring efforts. Furthermore, no damage is observed in specimen SY-3 during the two thermal fatigue stages, suggesting that welded regions are more susceptible to thermal fatigue damage and require focused monitoring.

5 Conclusion

To address the need for dynamic detection of thermal fatigue damage in heat transfer oil pipes, this study conducts experimental testing and damage monitoring using AE technology under simulated thermal fatigue loading. Three types of U-shaped specimens are designed based on the structural characteristics of heat transfer oil pipes. A thermal fatigue cycle loading device and insulation box are developed to replicate the actual inner-wall loading conditions. Thermal fatigue cycle tests are performed on the three specimens, with full process AE monitoring. After two stages of thermal fatigue loading, AE signals are detected from specimen SY-1 (both stages) and specimen SY-2 (second stage), while no signals are generated from specimen SY-3. X-ray detection validates the initiation and propagation of thermal fatigue cracks in specimens SY-1 and SY-2, confirming the effectiveness of AE technology in monitoring thermal fatigue damage.

Key findings indicate that crack initiation is more likely to occur during the heating stage, providing reliable data for in-service damage monitoring of heat transfer oil pipes. Welded regions are identified as high-risk areas for thermal fatigue damage, requiring prioritized monitoring. Future research will extend thermal fatigue cycle experiments to non-welded specimens, aiming to provide a reference for service life prediction of non-welded thermal fatigue damage.

Data availability statement

The raw data supporting the conclusions of this article will be made available by the authors, without undue reservation.

Author contributions

ZH: Data curation, Funding acquisition, Writing – original draft. XLu: Data curation, Investigation, Software, Writing – original draft. JZ: Methodology, Writing – review and editing, Validation. QL: Funding acquisition, Supervision, Validation, Writing – review and editing. CH: Validation, Writing – review and editing. CL: Supervision, Writing – review and editing. XLi: Methodology, Validation, Writing – review and editing.

Funding

The author(s) declared that financial support was received for this work and/or its publication. This work was supported in part by the National Key R&D Program (No.2024YFB3214300), National Natural Science Foundation of China (No. 92360304 and 12364056), Key Research and Development Program of Jiangxi Province (20253BAC280090,0252BAC240318), Science and Technology Program of CSEI (2024youth10).

Conflict of interest

The author(s) declared that this work was conducted in the absence of any commercial or financial relationships that could be construed as a potential conflict of interest.

Generative AI statement

The author(s) declared that generative AI was not used in the creation of this manuscript.

Any alternative text (alt text) provided alongside figures in this article has been generated by Frontiers with the support of artificial intelligence and reasonable efforts have been made to ensure accuracy, including review by the authors wherever possible. If you identify any issues, please contact us.

Publisher's note

References

1. Viebahn P, Lechon Y, Trieb F. The potential role of concentrated solar power (CSP) in Africa and europe—A dynamic assessment of technology development, cost development and life cycle inventories until 2050. *Energy Policy* (2011) 39:4420–30. doi:10.1016/j.enpol.2010.09.026

2. Zamorano M, Gómez MJ, Castejon C, Carboni M. Analysis of acoustic emission waveforms by wavelet packet transform for the detection of crack initiation due to fretting fatigue in solid railway axles. *Appl Sci* (2025) 15(15):8435. doi:10.3390/app15158435

3. Zheng Z, Li H, Zhang X, Jiang H, Geng X, Li S, et al. High-absorption solar steam device comprising Au@Bi2MoO6-CDs: extraordinary desalination and electricity generation. *Nano Energy* (2020) 68:104298. doi:10.1016/j.nanoen.2019.104298

4. Zhao X, He Z, Qu W, Lin P, Chen Y, Chen Y. Narrow-bandgap light-absorbing conjugated polybenzobisthiazole: massive interfacial synthesis, robust solar-thermal evaporation and thermoelectric power generation. *Sci China (Materials)* (2022) 65(09):2491–501. doi:10.1007/s40843-021-2002-1

5. Huang L, Deng J, Hu D, Li X, Liu Y, Zhu W. A comparative study of shear crack growth mechanisms in concrete through acoustic emission analysis. *Scientific Rep* (2025) 15(1):17272. doi:10.1038/s41598-025-01409-0

6. Vinod Ingle V, Prem PR. Acoustic emission examination of 3D printed ultra-high performance concrete with and without coarse aggregate under fresh and hardened states. *J Building Eng* (2025) 111:13491. doi:10.1016/j.jobe.2025.113491

7. Lean Tai J, Sultan MTH, Łukaszewicz A, Siemiątkowski Z, Skorulski G, Shahar FS. Preventing catastrophic failures: a review of applying acoustic emission testing in multi-bolted flanges. *Metals* (2025) 15(4):438. doi:10.3390/met15040438

8. Trush VS, Pochapskyi YP, Klym BP, Kravchyshyn TM, Tikhonovsky MA, Stoev PI, et al. Acoustic emission of Zr–1% Nb alloy with the modified surface layer under tension. *Mater Sci* (2025) 60(2):1–7. doi:10.1007/s11003-025-00872-4

9. Teng Z, Gao Z, Yu S, Yang Y. Detecting cradks with different depth-width ratio by array eddy current. *J. Fail. Anal. and Pre.* (2024) 19(1):20-23+61.

10. He Y, Qiu Y, Wang K, Yuan F, Wang WQ, Li MJ, et al. Perspective of concentrating solar power. *Energy* (2020) 198:117373. doi:10.1016/j.energy.2020.117373

11. Du B, He Y, Zheng Z, Cheng ZD. Analysis of thermal stress and fatigue fracture for the solar tower molten salt receiver. *Appl Therm Eng* (2016) 99:741–50. doi:10.1016/j.applthermaleng.2016.01.101

12. Janssens KGF. Random grid, three-dimensional, space-time coupled cellular automata for the simulation of recrystallization and grain growth. *Model Simul Mater Sci Eng* (2003) 11:157–71. doi:10.1088/0965-0393/11/2/304

13. Qi G. Attenuation of acoustic emission body waves in acrylic bone cement andsynthetic bone using wavelet time-scale analysis. *J Biomed MaterialsResearch* (2000) 52(1):148–56. doi:10.1002/1097-4636(200010)52:1<148::aid-jbm19>3.0.co;2-6

14. Jin H, Zhang J, Felix AC, Aroyave MH. Oxide/substrate interfacial defects in high temperature oxidation of Co-40Cr by acoustic emission method. *J Southeast University(English Edition)* (2006)(01) 125–9.

15. He K, Tan Z, Cheng Y, Xiao D, Zhang Z. Key issues in acoustic emission detection technology for welding solidification cracks. *J Hunan Univ Scienc e Technology (Natural Sci Edition)* (2015) 30(04):40–6.

16. Peng J, Qian Y, Yin W, Wang Q. Fracture mechanism and precursors of thermally damaged granite uniaxial compression based on acoustic emission information. *Chin J Eng* (2023) 45(12):2129–39. doi:10.13374/j.issn2095-9389.2022.10.21.006

17. Xu H, Gong S, Chen L, Zhang C. Failure mechanisms of thermal barrier coatings under thermo-mechanical coupling effects. *J Beihang Univ* (2004)(10) 919–24. doi:10.13700/j.bh.1001-5965.2004.10.003

18. Zhang L, Duan X, Long X, Yin L, Xie J. Molecular dynamics simulation of effects of thermal cycling and grain boundaries on the growth of whiskers in copper-tin coatings. *J. Fail. Anal. and Preven.* (2024) 19(03):186–193. doi:10.3969/j.issn.1673-6214.2024.03.006

19. Lin G, Cao J. Research on wavelet basis construction based on acoustic emission signal characteristics of gas pipeline leaks. *Vibrations and Shocks* (2023) 42(10):128–35.

20. Ju X, Liang Y, Zhao X, Yang J. Detection of fatigue cracks in steel bridges using acoustic emission technology. *J Harbin Eng Univ* (2023) 44(04):649–656.

21. Wei Q, Song P, Liu G, Li Z, Qu X. Method for identifying fatigue cracks in oil and gas pipelines on offshore platforms. *J Harbin Eng Univ* (2022) 43(04):481–7.

22. Jianchao L, He Q, Lü Y. Research progress in non-destructive testing technology of thermal barrier coatings. *China Surf Eng* (2019) 32(02):16–26.

23. Liu W, Chen J, Wang Q, Xu K, Shen J. Study on Evaluation Method of Steel Strand Tensile Damage Based on Wavelet Packet Decomposition. *J Nanchang Hangkong Univ (Nat Sci)* (2024) 38(01) 73–84. doi:10.3969/j.issn.2096-8566.2024.01.010

24. Shi D, Jiang Y, Lu Z, Zhang Z. Leakage detection method for LNG cryogenic storage tanks based on acoustic emission technology. *China Offshore Platform* (2025) 40(05):97–102. doi:10.12226/j.issn.1001-4500.2025.05.20250513

25. van Blokland J, Erives RI, Bangaru AK, McGugan M, Sørensen BF. Fracture resistance of wood adhesive bonds: experimental insights into the J-integral approach using acoustic emission testing. *IOP Conf Ser Mater Sci Eng* (2025) 1338(1):012005. doi:10.1088/1757-899x/1338/1/012005

26. Raeker EB, Tulshibagwale N, Mullin KM, Lamb JD, Pollock TM. Detection and classification of cracking *via* acoustic emission during laser-melting screening for additive manufacturing. *JOM* (2025) 77(10):1–13. doi:10.1007/s11837-025-07642-2

27. Qin R, Zhou R, Li Q, Lu C, Huang L. Acoustic emission source location method for glass fibre reinforced plastics based on virtual loading focusing enhancement technology. *Nondestructive Test Eval* (2024) 39:1250–65. doi:10.1080/10589759.2023.2252563

28. Sheehan J, Zhai Q, Chuang LY, Officer T, Wang Y, Zhu L, et al. Applying EQTransformer to laboratory earthquakes: detecting and picking acoustic emissions with machine learning. *Earth, Planets and Space* (2025) 77(1):116. doi:10.1186/s40623-025-02237-2

29. Shi C, Wen N, Ma G, He M, Chen Y. Effects of freeze-thaw cycles on granite failure using acoustic emission test. *J Rock Mech Geotechnical Eng* (2025) 17(7):4512–26. doi:10.1016/j.jrmge.2024.11.021

30. Xu C, Khan M, Daly M, Gonzalez Nunez M, Ozevin D. Detecting secondary to tertiary creep transitions by acoustic emission. *Measurement* (2025) 255:118096. doi:10.1016/j.measurement.2025.118096